Chemical Science

ROYAL SOCIETY OF CHEMISTRY

EDGE ARTICLE

View Article Online
View Journal | View Issue

Cite this: *Chem. Sci.*, 2023, **14**, 711

All publication charges for this article have been paid for by the Royal Society of Chemistry

Received 1st October 2022
Accepted 12th December 2022

DOI: 10.1039/d2sc05473f

rsc.li/chemical-science

Enantioselective inhibition of the SARS-CoV-2 main protease with rhenium(I) picolinic acid complexes†

Johannes Karges, [a] Miriam A. Giardini, [b] Olivier Blacque, [c] Brendon Woodworth, [d] Jair L. Siqueira-Neto[b] and Seth M. Cohen *[a]

Infections of the severe acute respiratory syndrome coronavirus 2 (SARS-CoV-2) have triggered a global pandemic with millions of deaths worldwide. Herein, the synthesis of functionalized Re(I) tricarbonyl complexes as inhibitors of the SARS-CoV-2 main protease, also referred to as the 3-chymotrypsin-like protease ($3CL^{pro}$), is presented. The metal complexes were found to inhibit the activity of the enzyme with IC_{50} values in the low micromolar range. Mass spectrometry revealed that the metal complexes formed a coordinate covalent bond with the enzyme. Chiral separation of the enantiomers of the lead compound showed that one enantiomer was significantly more active than the other, consistent with specific binding and much like that observed for conventional organic small molecule inhibitors and druglike compounds. Evaluation of the lead compound against SARS-CoV-2 in a cell-based infection assay confirmed enantiospecific inhibition against the virus. This study represents a significant advancement in the use of metal complexes as coordinate covalent inhibitors of enzymes, as well as a novel starting point for the development of novel SARS-CoV-2 inhibitors.

Introduction

The ongoing global pandemic of the severe acute respiratory syndrome coronavirus 2 (SARS-CoV-2) has caused millions of deaths worldwide and there is an urgent need for novel therapeutics.[1] Fortunately, effective vaccines have been developed that provide prophylactic protection from viral infection.[2,3] Despite the availability of these medical countermeasures, vaccination may not be an option for individuals with compromised immune systems or other severe conditions. In addition, viral mutations can undermine the effectiveness of vaccines.[4–6] As such, there remains a need for the development of therapeutics towards SARS-CoV-2 infections.

The 3-chymotrypsin-like protease ($3CL^{pro}$), which is also referred to as the main protease (M^{pro}), is considered one the most important viral targets for SARS-CoV-2. This protein is involved in the proteolytic cleavage of the SARS-CoV-2 polyproteins and is necessary for viral replication and transcription. Inhibition of this protease disrupts the viral life cycle and as such is an important target for therapeutic intervention.[7–9] Clinical studies have shown that patients infected with coronaviruses and treated with protease inhibitors had reduced symptoms and mortality.[10] A number of $3CL^{pro}$ inhibitors including Lopinavir, Ritonavir, ASC09F in combination with Oseltamivir, Darunavir in combination with Cobiscistat, or PF-07321332 in combination with Ritonavir are currently being investigated in clinical trials.[11–14]

In addition to these conventional, organic, small molecule drug candidates, some attention has also been devoted towards the development of metal complexes as potential SARS-CoV-2 inhibitors. Metal complexes can display a more 3-dimensional geometry than many comparably sized organic compounds, presenting the possibility for enhanced interactions with the target active site.[15,16] In addition, extensive studies by Meggers *et al.* and others have shown that the functionalization of bioactive organic molecules with an inert metal core can improve the affinity and selectivity of enzyme inhibitors.[17–21]

With respect to SARS-CoV-2, high-throughput screening (HTS) identified the organoselenium compound Ebselen as an inhibitor of SARS-CoV-2 infection in Vero E6 cells with low micromolar activity.[22] Based on these results, other studies have sought to optimize the activity of Ebselen toward SARS-CoV-2, but with limited success.[23–25] High-throughput screening studies by Ott *et al.* and others have demonstrated that gold complexes could protect CaCo-2 cells from infections with SARS-CoV-2.[26] Alternatively, $[Re(2,2'\text{-bipyridine})(CO)_3(H_2O)]^+$ complexes were shown to act as coordinate covalent $3CL^{pro}$

[a]*Department of Chemistry and Biochemistry, University of California, La Jolla, San Diego, California 92093, USA. E-mail: scohen@ucsd.edu*

[b]*Skaggs School of Pharmacy and Pharmaceutical Sciences, University of California, La Jolla, San Diego, California 92093, USA*

[c]*Department of Chemistry, University of Zurich, Winterthurerstrasse 190, CH-8057, Zurich, Switzerland*

[d]*Department of Medicine, Division of Infectious Diseases, University of California San Diego, La Jolla, California 92093, USA*

† Electronic supplementary information (ESI) available. CCDC 2205502–2205530. For ESI and crystallographic data in CIF or other electronic format see DOI: https://doi.org/10.1039/d2sc05473f

inhibitors. Mass spectrometry analysis showed that loss of the water ligand and formation of an single [Re(2,2′-bipyridine)$(CO)_3]^+$ adduct by coordinate covalent binding to $3CL^{pro}$. The best Re(I) compounds from this prior report (where the complex possesses different substituents on the bipyridine ligand) were found to display inhibitory activity against $3CL^{pro}$ with IC_{50} values in the low micromolar range.[27] In this context it is important to highlight that Re complexes, and in particular Re(I) tricarbonyl complexes, are generally considered to be kinetically inert, allowing for their potential use in biological settings. Several compounds have been studied as potential enzyme inhibitors, anticancer, antibacterial, and antifungal agents. Studies have revealed that these metal complexes typically act through non-classical mechanisms of action.[28–31]

In this report, [Re(picolinic acid)$(CO)_3(H_2O)$] complexes are described as inhibitors of $3CL^{pro}$. Over 40 derivatives of the [Re(picolinic acid)$(CO)_3(H_2O)$] motif were synthesized and characterized (where the complex possesses different substituents on the picolinic acid ligand), and their *in vitro* activity towards $3CL^{pro}$ investigated. Mass spectrometry verified the formation of a single covalent adduct between the metal complex and the enzyme target. The lead compounds were found to have a high selectivity for $3CL^{pro}$ when tested against other human proteases and other SARS-CoV-2 associated enzymes. Enantioselective separation of the lead compound isomers revealed that one stereoisomer shows good activity towards the target enzyme, while the other isomer is essentially inactive. Antiviral studies show that the active isomer can protect infected cells from SARS-CoV-2 in cell culture.

Results and discussion

Synthesis and characterization

Methyl-, carboxylic acid-, amine-, and hydroxy-functionalized picolinic acid (pic) ligands were purchased. The chloropicolinic acids were synthesized from the hydroxypicolinic acids with phosphoryl chloride. Upon further treatment with a palladium catalyst and silver(I) fluoride, the chloropicolinic acids could be converted to fluoropicolinic acids. The chloride moiety could also be substituted with a trifluoromethyl group upon reaction with copper(I) iodide and methyl fluorosulfonyldifluoroacetate. The fluoropicolinic acids were used in a reaction with potassium cyanide to introduce a cyano functionality. Methoxy-substituted picolinic acids were prepared from the hydroxy-derivatives by treatment with iodomethane. Finally, the nitro-functionalized picolinic acids were synthesized from the corresponding methyl-nitropyridines upon oxidation of the methyl group to the carboxylic acid with potassium permanganate. Synthetic details for all of these procedures can be found in the ESI.†

The synthesis of the Re(I) tricarbonyl complexes **1**,[32,33] **17**,[32,34] and **27** (ref. 34,35) have been previously described, while compounds **2–16**, **18–26**, **28–41** are, to the best of our knowledge, reported here for the first time (Fig. 1). The synthesis of these compounds starts with pentacarbonylchlororhenium(I). Upon heating of the Re(I) compound at reflux in acetonitrile, two equivalents of carbon monoxide are released and replaced by solvent molecules. Following this, the reaction solvent is changed to water and the respective picolinic acid derivative added. Upon heating of the Re(I) precursor with the ligand at

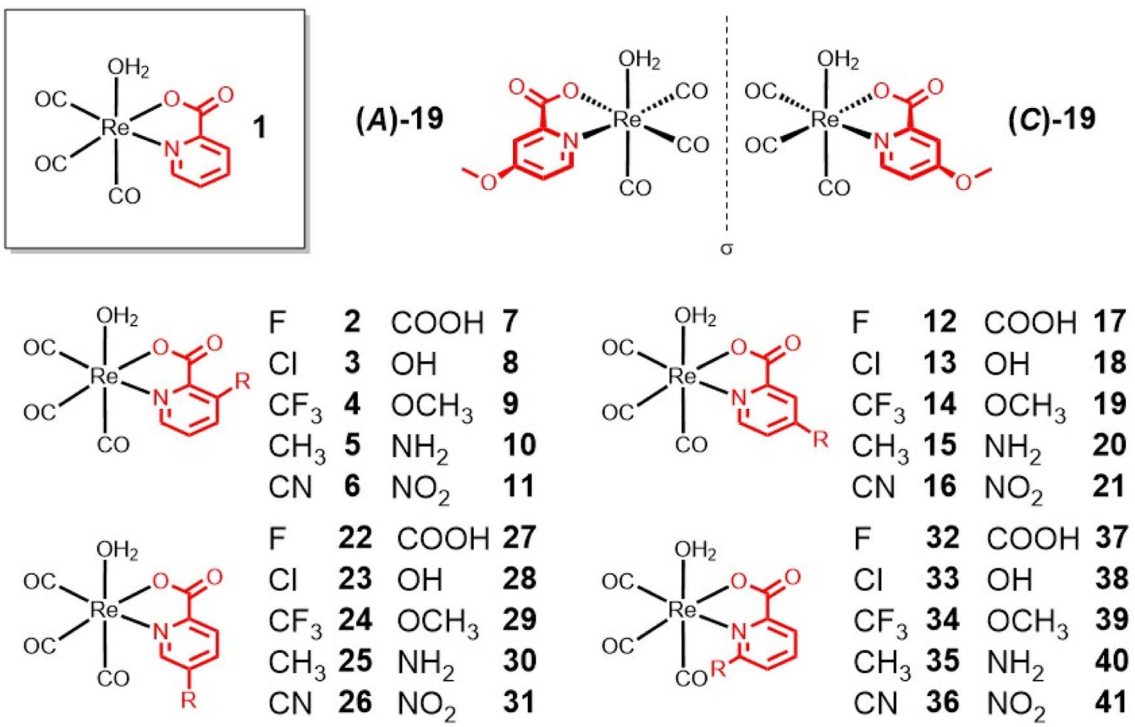

Fig. 1 Chemical structures of Re(I) tricarbonyl complexes investigated in this study.

reflux, metal complexes **1–41** (Fig. 1) were formed within a few hours and were isolated by recrystallization from water at reduced temperature. All picolinic acids as well as Re(I) tricarbonyl complexes were characterized by ^{1}H- and ^{13}C-NMR spectroscopy as well as high-resolution mass spectrometry. Purity of the final compounds was verified by HPLC analysis (Fig. S1–S6†).

The molecular structures of the investigated Re(I) tricarbonyl complexes **2–5**, **8–13**, **15**, **19**, **22–26**, **29–30**, **32–39**, and **41** were confirmed by single crystal X-ray diffraction studies (Fig. S7–S9 and Tables S1–S15†). Representative examples of these structures, specifically of compounds with substituents at the 4-position of the picolinic acid ligand, are shown in Fig. 2. The crystal structures of complex **1** [32] and **17** [34] have been previously reported. As expected, in all of these structures, the rhenium center is chelated by pic through the nitrogen atom and one oxygen atom of the carboxylic acid group, and bound by three carbonyl ligands and a water molecule. The water molecule is in a *trans* position to a carbonyl group, while the two other carbonyl groups are in *trans* positions to the chelating pic ligand. All bond distances and angles fall in typical ranges. The bond distances Re–O_{water} and Re–O_{pic} are found in the narrow range of 2.171(3) – 2.205(3) Å (values from structures **31** and **11**, respectively) and 2.114(2) – 2.168(3) Å (**9** and **15**, respectively). The size of the N^O pincer of the picolinic acid does not vary much in the structures, with the smallest angle of 73.98(8)° in **32** to the largest angle of 75.91(10)° in **8**. The metal center exhibits a distorted octahedral geometry in all structures and the N_{pic}–Re–O_{water} and O_{pic}–Re–O_{water} bond angles are significantly smaller than 90° (between 76.96(11) and 84.89(14)° in **4** and **15**, respectively). The N_{pic}–Re–C_{CO} and O_{pic}–Re–C_{CO} bond angles (the carbonyl group *trans* to the water molecule) are larger than 90° in the range 91.96(9) – 97.88(13) Å (**13** and **25**, respectively). The influence of the substitution on the picolinic acid is very limited with respect to the overall coordination geometry of the molecules; however, it is worth noting that the Re–N_{pic} bond length is significantly longer when the substituent is in the 6-position of the picolinic acid ligand (2.196(3) – 2.265(2) Å; **38** and **34**, respectively) when compared with substitution at the 3-, 4-, or 5-positions (2.162(2) – 2.190(3) Å; **10** and **30**, respectively). This difference is likely due to a steric hindrance between the substituent and the nearest carbonyl group.

The aqueous solubility of a compound is an important consideration for any bioactive molecule. The [Re(pic)$(CO)_3$(H_2O)] complexes generally showed poor water solubility; therefore, stock solutions of these were prepared in dimethyl sulfoxide (DMSO) or dimethylformamide (DMF) and diluted for the studies reported herein. Previous studies on metallodrugs have indicated that the therapeutic effect of a metal complex can be altered by interactions with DMSO.[36,37] To investigate if this was the case for these Re(I) compounds, complex **1** (as a representative of the class) was dissolved in DMSO-d_6 the aqua ligand exchange in [Re(pic)$(CO)_3$(H_2O)] was followed by ^{1}H-NMR spectroscopy. Within 5 min, two sets of signals were observed in the ^{1}H-NMR spectra, indicating rapid exchange of the aqua ligand with DMSO. Over the course of 70 min, the signals for [Re(pic)$(CO)_3$(H_2O)] steadily decreased and were replaced by the signals for [Re(pic)$(CO)_3$(DMSO)] (Fig. S10†). To confirm these observations, the DMSO complexes of **1**, referred to as $\mathbf{1_{DMSO}}$, was directly synthesized and isolated. The aqueous stability of the DMSO adduct $\mathbf{1_{DMSO}}$ was studied by ^{1}H-NMR spectroscopy by incubation in 2 : 8 DMSO-d_6 : H_2O. While the emergence of two sets of signals, corresponding to the aqua and DMSO coordinated metal complexes, was observed after 2 h, the majority of the compound remained as the DMSO adduct even after 6 h (Fig. S11†). These findings indicate the reversibility of the solvent coordination in axial position. Following the adduct formation with DMSO, the interaction with DMF was studied. Complex **1** was dissolved in DMF-d_7 and the coordination of the solvent was followed by ^{1}H-NMR spectroscopy. Upon incubation for 60 min, an emerging set of signals corresponding to [Re(pic)$(CO)_3$(DMF)] was observed. Following longer incubation times, the signals for [Re(pic)$(CO)_3$(H_2O)] steadily decreased and were replaced by the signals for [Re(pic)$(CO)_3$(DMF)]. Within 6 h the axial ligand was fully exchanged (Fig. S12†). To assess the solubility of these compounds in an aqueous solution, compound **1** was dissolved in 0.4–0.1% DMSO or DMF in phosphate-buffered saline solutions and formation of any precipitates was monitored by dynamic light scattering (DLS) measurements. No particle formation or aggregation was observed, suggesting sufficient aqueous solubility of the metal complexes under these solution conditions. To assess the stability of these metal complexes under physiological conditions, compound **1** (1% DMF) was incubated in water or phosphate-buffered saline for 24 h and analyzed by HPLC. No

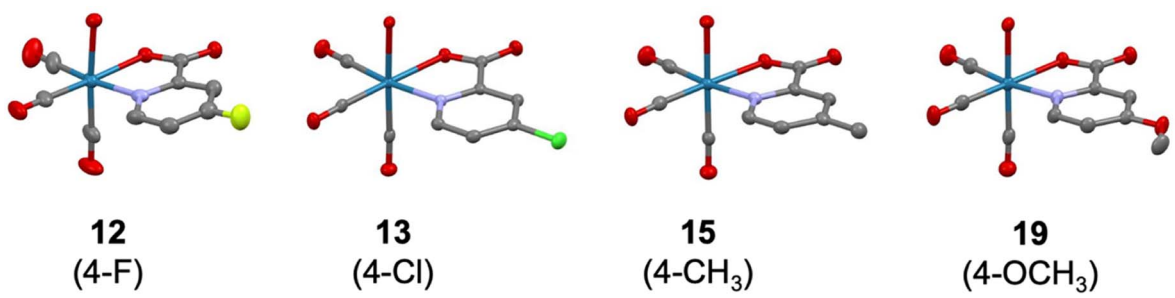

Fig. 2 Single crystal X-ray diffraction structures (50% probability ellipsoids) of [Re(pic)$(CO)_3$(H_2O)] complexes with substituents in the 4-position of the picolinic acid (pic) ligand. Hydrogen atoms and co-crystallized solvent molecules are omitted for clarity.

changes in the chromatogram were observed (Fig. S13†), suggesting stability of these Re(I) tricarbonyl complexes in an aqueous solution. Overall, these results indicate the suitability of these stock solutions for use in experiments under biologically relevant conditions. The majority of the studies described below were performed from DMF stock solutions of the compounds.

Coordinate covalent binding

To investigate the interaction of the Re(I) complexes with the target protein $3CL^{pro}$, compound **1** (as a representative example) was incubated with the enzyme. After incubation for 2 h, the mixture was analyzed by liquid chromatography electrospray ionization time-of-flight mass spectrometry (ESI-TOF-MS). While the enzyme itself was found with a deconvoluted mass of 33 797 Da (Fig. 3a), upon incubation with the Re(I) tricarbonyl complex the peak shifted to 34 191 Da (Fig. 3b), corresponding to a single attached metal complex ($\Delta m/z$ 393 Da). As a complementary method, the binding of the metal complex to $3CL^{pro}$ was studied by inductively coupled plasma mass spectrometry (ICP-MS). Compound **1** was incubated with $3CL^{pro}$ for 2 h, followed by washing of the protein to remove any unbound metal complexes, and digestion of the resulting sample with nitric acid. The Re content was analyzed by ICP-MS, giving a value of 0.7 ± 0.2 equivalents of Re per $3CL^{pro}$ (see ESI† for details), which is generally consistent with the mass spectrometric analysis.

To get some insight into the binding of **1** to $3CL^{pro}$, computational experiments were performed. The 3-dimensional geometry of the metal complex was optimized by density functional theory (DFT) calculations. After DFT optimization, the compound was docked to the structure of $3CL^{pro}$. For the docking simulations, the water molecule that acts as a capping ligand was removed to the generate a metallofragment that was then evaluated against cysteine residues found in $3CL^{pro}$. The generated poses were energetically minimized and scored using the GBVI/WSA dG force field. The lowest energy pose indicated that the Re(I) tricarbonyl complex was bound to Cys145 (Fig. 3c), which is the catalytically active Cys residue in $3CL^{pro}$. In an attempt to experimentally elucidate the binding site of compound **1**, $3CL^{pro}$ was first incubated with GC376, which has been unambiguously characterized by macromolecular

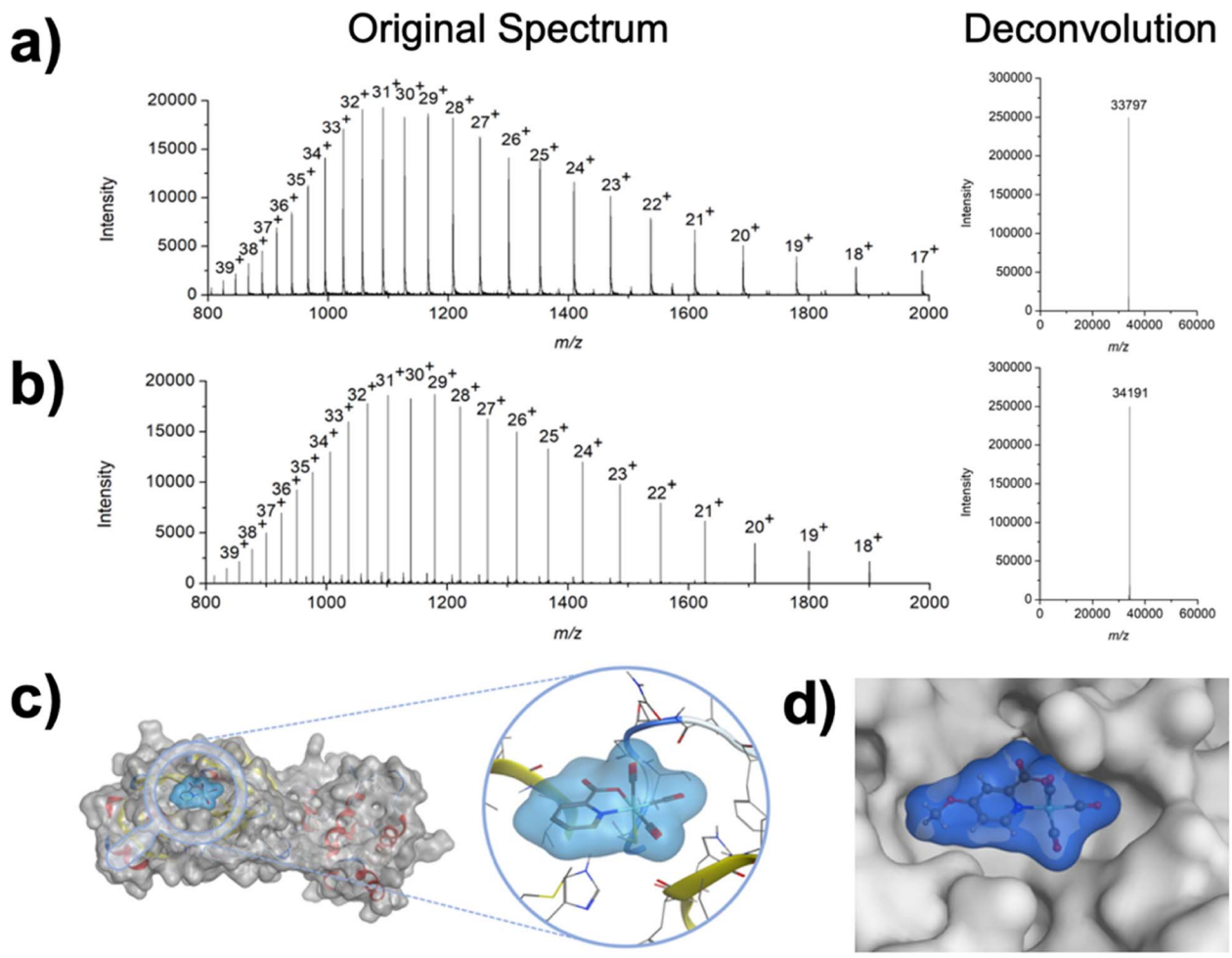

Fig. 3 Original and deconvoluted mass spectrum of: (a) $3CL^{pro}$ and (b) $3CL^{pro}$ upon incubation with **1**. (c) Computationally predicted binding pose of the [Re(pic)(CO)$_3$] fragment bound to the thiol group of Cys145 of $3CL^{pro}$. (d) Computationally predicted binding pose of the **(*A*)-19** fragment bound to the thiol group of Cys145 of $3CL^{pro}$.

crystallography to bind to the catalytic Cys145 residue in the active site of 3CL^{pro}.[38] As expected, incubation with the covalent inhibitor GC376 generated a new enzyme adduct with a mass of 34 201 Da (Fig. S14†), corresponding to a single GC376 covalent adduct (Δ*m*/*z* 404 Da). After reaction with GC376, the GC376-3CL^{pro} adduct was treated with compound **1**. ESI-TOF did not show the formation of new products, but only the presence of the GC376-3CL^{pro} adduct (Fig. S15†), suggesting that the metal complex targets the same amino acid. Similar results were obtained upon incubation of [Re(2,2′-bipyridine)(CO)$_3$(H$_2$O)]$^+$ with the GC376-3CL^{pro} adduct.[27] In both cases, these findings suggest that these Re(I) compounds bind to Cys145 in the active site of the protein; however, the Cys44 residue is also proximal to the active site of 3CL^{pro}. Attempts to unambiguously determine the site of binding for compound **1** (*via* macromolecular X-ray crystallography or protein digestion mass spectrometry) have not been successful to date, and as such binding of these complexes to the Cys44 residue cannot be unambiguously ruled at this time. Overall, these findings are most consistent with compound **1** generating a coordinate covalent interaction at Cys145 in the active site of 3CL^{pro}.

Inhibition against 3CL^{pro}

After confirmation of the covalent adduct formation of **1** with 3CL^{pro} by mass spectrometry, the inhibitory activity of the [Re(pic)(CO)$_3$(H$_2$O)] derivatives was investigated against 3CL^{pro}. Compounds **1–41** were incubated with 3CL^{pro} at a concentration of 100 μM and the activity of the protein assessed in a fluorescence-based assay (see ESI† for details). The activity of the [Re(pic)(CO)$_3$(H$_2$O)] derivatives against 3CL^{pro} at a compound concentration of 100 μM is summarized in Table 1. The screening of compounds **1–41** at 100 μM showed a clear preference for the position of the substituent on the picolinic acid ligand. Substituents at the 3-position (**3–11**) were not tolerated, with the exception of fluoride (**2**). Substituents at the 4-position gave more varied results depending on the functional group, with the majority of groups not tolerated (**12–17**, **21**), but hydroxy, methoxy, or amine groups (**18–20**) giving good activity. By contrast, substituents in the 5- and 6-positions (**21**, **28–30**, **32–33**, **35–41**) were well tolerated, with some exceptions including chloride, trifluoromethyl, carboxylic acid, and nitro (**23–27**, **31**, **33**, **34**, **37**, **41**) (Table 1).

Following this preliminary, single-point screening, the half maximal inhibitory concentration (IC$_{50}$) values of compounds that showed an inhibitory activity of >80% at 100 μM were determined (Table 2, Fig. S16 and S17†). Compounds with substituents at the 5- and 6-positions (**28–30**, **32**, **35–36**, **38–40**) were found not to improve the inhibitory activity in comparison to the unsubstituted compound **1**. The inhibitory activity of the [Re(pic)(CO)$_3$(H$_2$O)] complexes that were functionalized in the 4-position showed activity that was dependent on the functional group. The modification of the ligand scaffold with a hydroxy

Table 1 Color-coded summary of the enzymatic activity of the [Re(pic)(CO)$_3$(H$_2$O)] complexes **1–41** at a concentration of 100 μM against 3CL^{pro}. Standard deviations are given in parentheses. Cells are color-coded by percent inhibition: white (<20%), yellow (20–80%), red (>80%)

	% inhibition 3CL^{pro}		% inhibition 3CL^{pro}		% inhibition 3CL^{pro}
1	93 (4)	**15**	38 (7)	**29**	83 (6)
2	87 (6)	**16**	14 (8)	**30**	86 (5)
3	25 (8)	**17**	11 (8)	**31**	17 (7)
4	2 (4)	**18**	89 (7)	**32**	93 (5)
5	22 (6)	**19**	81 (6)	**33**	26 (6)
6	12 (7)	**20**	87 (7)	**34**	28 (5)
7	8 (5)	**21**	8 (6)	**35**	86 (6)
8	5 (7)	**22**	75 (8)	**36**	92 (7)
9	13 (6)	**23**	24 (8)	**37**	31 (8)
10	7 (4)	**24**	8 (9)	**38**	89 (5)
11	17 (7)	**25**	15 (7)	**39**	86 (7)
12	41 (5)	**26**	37 (7)	**40**	84 (6)
13	11 (7)	**27**	9 (6)	**41**	11 (8)
14	4 (6)	**28**	85 (7)		

Table 2 IC_{50} values of select compounds against $3CL^{pro}$. Values and standard deviations are derived from three independent experiments. The organic covalent inhibitor GC376 was used as a reference

Compound	IC_{50} (μM)
1	9.1 ± 1.8
2	19.0 ± 3.7
18	4.6 ± 0.5
19	3.3 ± 0.4
20	8.4 ± 2.2
28	8.9 ± 1.9
29	8.6 ± 1.7
30	9.5 ± 2.4
32	9.4 ± 3.3
35	9.6 ± 3.1
36	8.9 ± 2.8
38	8.8 ± 3.4
39	8.5 ± 1.9
40	10.9 ± 3.1
GC376	0.14 ± 0.02

group (compound **18**, IC_{50} = 4.6 ± 0.5 μM) or a methoxy group (compound **19**, IC_{50} = 3.3 ± 0.4 μM) showed improved inhibitory activity with IC_{50} values that were 2- to 3-fold better than the unsubstituted [Re(pic)$(CO)_3(H_2O)$] (compound **1**, IC_{50} = 9.1 ± 1.8 μM). These findings suggest that the ligand scaffold could be further modified to enhance activity against $3CL^{pro}$ (Table 2).

Selectivity against human proteases and SARS-CoV-2 associated enzymes

To evaluate target selectivity, lead compounds **1**, **18**, and **19** were tested against a series of human proteases, including dipeptidyl peptidase-4 (DPP4, serine protease), Furin (serine protease), transmembrane serine protease 2 (TMPRSS2, serine protease), beta-secretase 1 (BACE1, aspartate protease), cathepsin B (cysteine protease), cathepsin L (cysteine protease), and SARS-CoV-2 Papain-like protease (PL^{pro}) using fluorescence-based assays (see ESI† for details). Encouragingly, complexes **1**, **18**, and **19** did not show measurable activity against DPP4, cathepsin B, Furin, PL^{pro} (IC_{50} > 100 μM), and showed only a weak effect on BACE-1 (IC_{50} = 76–94 μM) and cathepsin L (IC_{50} = 53–72 μM). This preliminary screen shows that the [Re(pic)$(CO)_3(H_2O)$] complexes can achieve some degree of selective inhibition against $3CL^{pro}$ over human proteases (Table 3).

Enantioselective inhibition against $3CL^{pro}$

Due to the asymmetric nature of the picolinic acid ligands used, the Re(I) metal complexes studied here were isolated as a racemic mixture of enantiomers. Several studies on the functionalization of the natural product staurosporine with metal fragments have demonstrated the importance of enantiomeric purity of metal complexes on their biochemical activity.[39,40] Therefore the enantiomers of **19** were separated by converting them into diastereomers through replacement of the axial aqua ligand with *N*-(*tert*-butoxycarbonyl)-L-cysteine methyl ester. The diastereomers were individually isolated by column chromatography and then treated with the cysteine selective scavenger 1-phenylprop-2-en-1-one (see ESI† for details). Upon removal of the cysteine adduct, the enantiopure, aqua complexes of **19** were regenerated and isolated (Fig. 4a). Notably, the isolation of enantiomerically pure Re(I) tricarbonyl complexes remains rare, although it has been previously achieved using chiral column chromatography[41] or a stereochemical directing ligand.[42] Using circular dichroism (CD) spectroscopy, the chiral isomers were characterized (Fig. 4b). To identify which enantiomer corresponds to which spectrum, density functional theory (DFT) calculations were performed and the CD spectrum calculated (Fig. S18†). The metal complexes were named following the rules of Cahn, Ingold, and Prelog[42] as enantiomers **(*A*)-19** and **(*C*)-19** based on the priority of the coordinated atoms. With the enantiopure compounds in hand, their ability to inhibit $3CL^{pro}$ was studied. Strikingly, **(*C*)-19** enantiomer showed poor activity (IC_{50} = 57 ± 9 μM), while the **(*A*)-19** enantiomer demonstrated excellent inhibition (IC_{50} = 1.8 ± 0.3 μM). The IC_{50} value of the **(*A*)-19** enantiomer was found to be almost exactly half of IC_{50} value of the racemic mixture (**19**, IC_{50} = 3.3 ± 0.4 μM), which is what would be expected for a racemic mixture containing one inactive and one active enantiomer (Fig. 4c). The ability of the separated enantiomers to form a coordinate covalent interaction with $3CL^{pro}$ was investigated by protein ESI-TOF-MS. Upon incubation of $3CL^{pro}$ with the active enantiomer **(*A*)-19**, the deconvoluted mass peak shifted to 34 219 Da (Fig. 4d), corresponding to a single metal complex adduct (Δ*m*/*z* 423 Da). In contrast, no change in the mass spectrum upon incubation of $3CL^{pro}$ with the inactive enantiomer **(*C*)-19** was observed (Fig. S19†). For a better understanding of the enantioselectivity of the metal complex, docking studies were performed. In comparison to the unfunctionalized metal complex **1** (Fig. 3c), the computational model showed that the methoxy group in the **(*A*)-19** enantiomer can occupy a subpocket of the active site (Fig. 3d). By contrast, the docking experiment suggested that the **(*C*)-19** enantiomer could not bind to $3CL^{pro}$. This is likely attributed to the steric hindrance of the substituted pic ligand. These findings are consistent with the enantiospecific binding observed in the enzymatic assay.

Table 3 Half maximal inhibitory concentration (IC_{50}, μM) of **1**, **18**, and **19** against $3CL^{pro}$, human proteases, and SARS-CoV-2 associated enzymes. Values and standard deviations are derived from three independent experiments

	1	**18**	**19**
$3CL^{pro}$	9.1 ± 1.8	4.6 ± 0.5	3.3 ± 0.4
DPP4	>100	>100	>100
BACE1	83 ± 6	76 ± 8	94 ± 5
Cathepsin B	>100	>100	>100
Cathepsin L	53 ± 7	67 ± 9	72 ± 7
PL^{pro}	>100	>100	>100
Furin	>100	>100	>100
TMPRSS2	>100	>100	>100

Antiviral activity against SARS-CoV-2 infected cells

Due to the encouraging inhibitory activity and selectivity for $3CL^{pro}$, antiviral studies in SARS-CoV-2 infected human cells

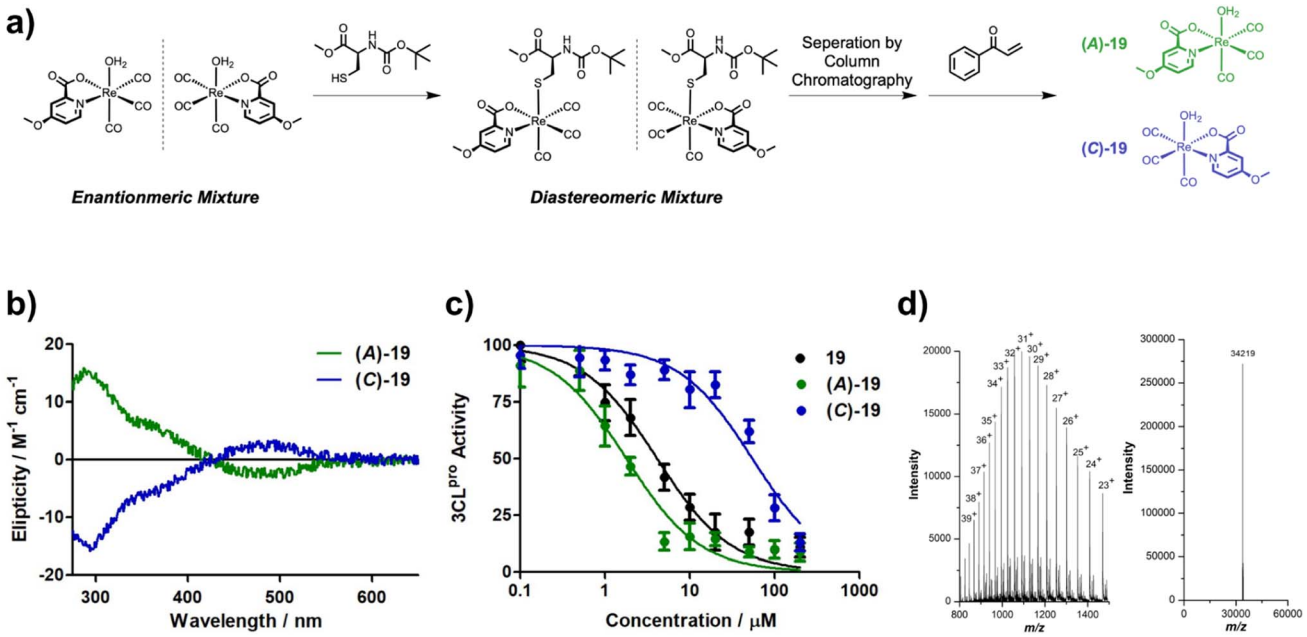

Fig. 4 Evaluation of the chiral enantiomers of compound **19**. (a) Synthetic strategy for separation of the enantiomers. (b) Circular dichroism spectra of the enantiomers **(A)-19** and **(C)-19** in methanol. (c) Dose–response curves of **19**, **(*A*)-19**, and **(*C*)-19** against $3CL^{pro}$. (d) Original and deconvoluted mass spectrum of $3CL^{pro}$ upon incubation with **(*A*)-19**.

were sought. Because DMSO stock solutions of compounds are commonly used for an evaluation in a cellular setting, the inhibitory activity of $\mathbf{1_{DMSO}}$ and $\mathbf{19_{DMSO}}$ against $3CL^{pro}$ was investigated. The DMSO-adducts were found to have a slightly decreased inhibitory activity ($\mathbf{1_{DMSO}}$, $IC_{50} = 16.5 \pm 3.4$ μM; $\mathbf{19_{DMSO}}$, $IC_{50} = 6.2 \pm 1.1$ μM) compared to their corresponding aqua complexes. While the activity of the DMSO complexes was reduced, the compounds remained active against $3CL^{pro}$. For a deeper understanding of the effects of the coordinated DMSO molecule, the inhibitory activity of $\mathbf{1_{DMSO}}$ in comparison to **1** was studied in a time dependent fashion. While the extending the preincubation time of **1** did not significantly change the activity against $3CL^{pro}$, extension of the preincubation time with $\mathbf{1_{DMSO}}$ showed a strongly enhance the inhibitory activity over time, due to slow aquation of the metal complex (Fig. S20†).

The antiviral activity of $\mathbf{1_{DMSO}}$, $\mathbf{19_{DMSO}}$, **(*A*)-$\mathbf{19_{DMSO}}$**, and **(*C*)-$\mathbf{19_{DMSO}}$** was tested towards SARS-CoV-2 infected African green monkey kidney (Vero E6) cells and hepatocyte-derived carcinoma (Huh 7.5.1) cells. The Re(I) complexes studied here were found to be non-toxic in Vero E6 cells and only mildly cytotoxic against Huh 7.5.1 cells, permitting evaluation of their antiviral activity. Vero E6 cells do not express the TMPRSS2 receptor, allowing viral entry only through cathepsin L mediated lysosomal uptake. By contrast, Huh 7.5.1 cells poorly express cathepsin L, but highly express the TMPRSS2 receptor, making TMPRSS2 the primary viral internalization pathway for this cell line.[43] The effect of the expression of the cellular entry receptors on the antiviral activity is highlighted by the compound K777.[44] K777 is a highly active and selective covalent inhibitor of cathepsin L. As such, K777 is able to protect Vero E6 from SARS-CoV-2, but is ineffective at protecting Huh 7.5.1 cells from SARS-CoV-2 infection.[44] Remdesivir interacts through inhibition of the SARS-CoV-2 RNA-dependent RNA polymerase[45] and as such is protective in both cell lines (Table 4).[46,47] Assuming the metal complexes interact through inhibition of $3CL^{pro}$, these compounds should show similar antiviral activity in both cell lines. Indeed, protective antiviral activity was found in both cell lines for $\mathbf{1_{DMSO}}$ and $\mathbf{19_{DMSO}}$. Notably, the antiviral activity in Huh 7.5.1 is somewhat inflated due to the weak cytotoxicity of the compounds in this cell line. Strikingly, **(*A*)-$\mathbf{19_{DMSO}}$** was found to be highly active, while **(*C*)-$\mathbf{19_{DMSO}}$** demonstrated poor antiviral activity in both cell lines (Table 4, Fig. S21 and S22†), consistent with their disparate *in vitro* activity (Fig. 4). The most potent metal complex **(*A*)-$\mathbf{19_{DMSO}}$** demonstrated a good antiviral

Table 4 Half maximal effective concentration (EC_{50}, μM) and half maximal cytotoxic concentration (CC_{50}, μM) of $\mathbf{1_{DMSO}}$, $\mathbf{19_{DMSO}}$, **(*A*)-$\mathbf{19_{DMSO}}$**, **(*C*)-$\mathbf{19_{DMSO}}$**, remdesivir, and K777 towards SARS-CoV-2 infected Vero E6 and Huh 7.5.1 cells. Values and standard deviations are derived from three independent experiments. A selectivity index (SI) has been calculated as CC_{50}/EC_{50}

	Vero E6			Huh 7.5.1		
	EC_{50}	CC_{50}	SI	EC_{50}	CC_{50}	SI
$\mathbf{1_{DMSO}}$	5.5 ± 0.7	>20	>9	1.8 ± 0.5	16.5 ± 1.3	9
$\mathbf{19_{DMSO}}$	2.2 ± 1.1	>50	>23	0.8 ± 0.2	14.8 ± 1.5	19
(*A*)-$\mathbf{19_{DMSO}}$	1.0 ± 0.3	>50	>50	0.7 ± 0.2	15.5 ± 1.2	22
(*C*)-$\mathbf{19_{DMSO}}$	>50	>50	—	7.1 ± 1.4	13.2 ± 1.7	2
Remdesivir	5.0 ± 0.8	>20	>4	<0.04	>20	>500
K777	0.009 ± 0.002	>2	>222	>2	>2	—

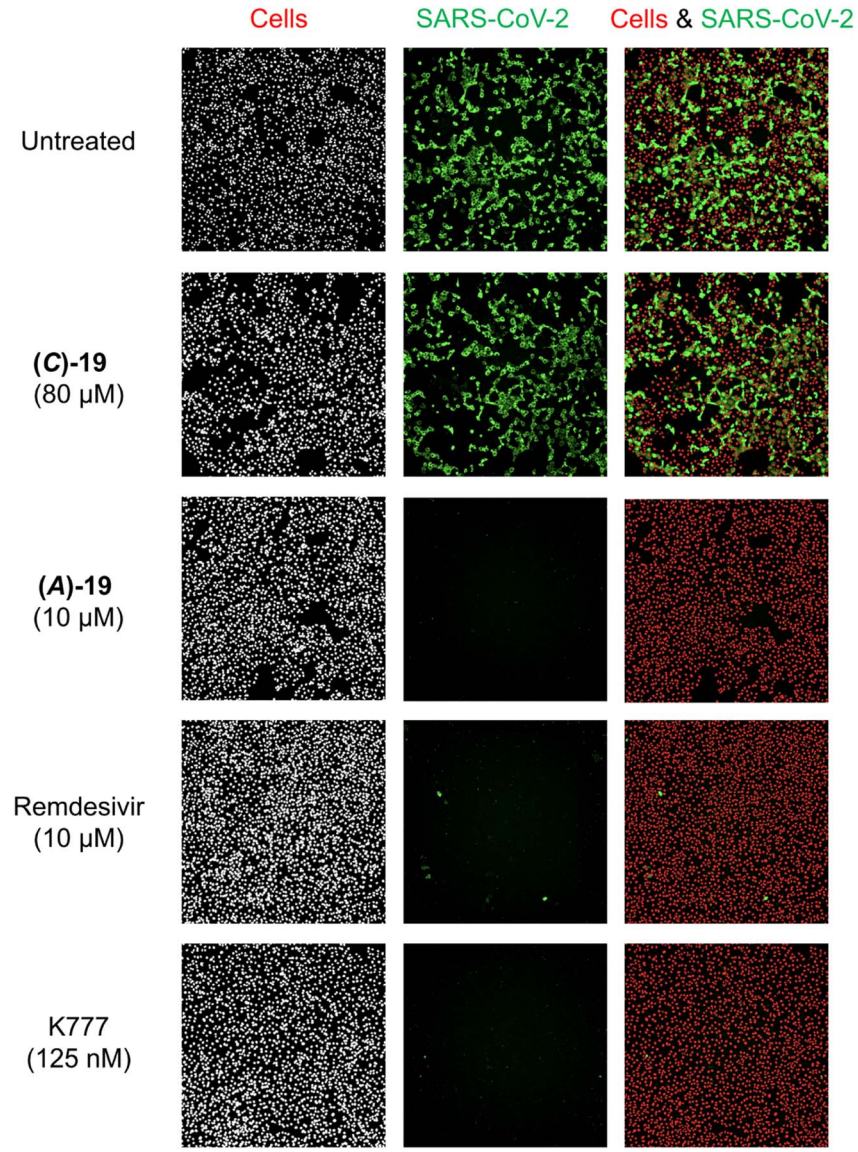

Fig. 5 Immunofluorescence microscopy images of SARS-CoV-2 infected Vero E6 cells treated with (*A*)-19 and (*C*)-19 and the control compounds remdesivir and K777. The nucleus of the cells was stained with 4′,6-diamidino-2-phenylindole (DAPI). The infection with SARS-CoV-2 was visualized with a SARS-CoV-2 selective antibody.

effect ($EC_{50,Vero\ E6} = 1.0 \pm 0.3$ μM; $EC_{50,Huh\ 7.5.1} = 0.7 \pm 0.2$ μM) resulting in therapeutic indices of >50 for Vero E6 cells and ~22 for Huh 7.5.1 cells (based on the measured cytotoxicity of **(*A*)-19$_{DMSO}$**, Table 4).

Using immunofluorescence microscopy, the antiviral effects of **(*A*)-19$_{DMSO}$**, **(*C*)-19$_{DMSO}$**, and control compounds remdesivir and K777 were visualized in Vero E6 cells. Treatment with K777 protected cells from viral infection at concentrations as low as 125 nM (Fig. 5). Treatment with **(*A*)-19$_{DMSO}$** at 10 μM also completely eradicated the viral infection, comparable to the effect of remdesivir at the same concentration (Fig. 5). By contrast, treatment with **(*C*)-19$_{DMSO}$** at a higher concentration of 80 μM did not provide protection against SARS-CoV-2. These findings are consistent with the measured IC_{50} values (*vide infra*, Fig. 4) and highlight the importance of the chirality of the metal complex.

Conclusions

In summary, this study reports on the synthesis and characterization of Re(I) tricarbonyl picolinic acid complexes as inhibitors of the SARS-CoV-2 main protease. Using mass spectrometry the coordinate covalent interaction of [Re(pic)$(CO)_3$(H_2O)] to the active site of to $3CL^{pro}$ was verified. A rudimentary SAR revealed that substitution with a methoxy group in 4-position of the picolinic acid ligand enhanced the inhibitory activity against $3CL^{pro}$ by ~3-fold. The metal complex was found to be selective for $3CL^{pro}$ over several human proteases and SARS-CoV-2 associated enzymes. The enantiomers of **19** were separated by formation of diastereomers *via* aqua ligand substitution, followed by re-aquation to isolate the resolved enantiopure complexes of **19**. Strikingly, while the **(*C*)-19**

enantiomer was found to be a poor inhibitor of $3CL^{pro}$ (IC_{50} = 57 ± 9 μM), the **(*A*)-19** enantiomer was determined to be highly active (IC_{50} = 1.8 ± 0.3 μM) against $3CL^{pro}$. These findings indicate the importance of the stereochemistry of the metal centre of these metallodrug fragment leads.

Data availability

The data that support the findings of this study are available in the ESI of this article.†

Author contributions

Synthesis and biochemical evaluation of the compound was performed by J. K. Biological evaluation was performed by M. A. G. and B. W. Crystal structure analysis was performed by O. B. The cell based studies were designed and supervised by J. L. S.-N. S. M. C. supervised the overall project, advised on experimental design and data interpretation, and guided manuscript preparation and editing.

Conflicts of interest

S. M. C. is a cofounder of and has an equity interest in Cleave Therapeutics, Forge Therapeutics, and Blacksmith Medicines, companies that may potentially benefit from the research results. S. M. C. also serves on the Scientific Advisory Board for Blacksmith Medicines and serves on the Scientific Advisory Board and receives compensation from Forge Therapeutics. The terms of this arrangement have been reviewed and approved by the University of California, San Diego in accordance with its conflict-of-interest policies.

Acknowledgements

This work was supported by National Institute of Health grant R01 AI149444. The authors acknowledge the support of Dr Yongxuan Su (U. C. San Diego, Molecular Mass Spectrometry Facility) for ESI-MS measurements, and support from the UCSD Screening Core and Trans Virology Core. The authors thank Jeewon Chung and Ryjul Stokes for verifying these studies by reproducing several of the synthesis, characterization, assay, and mass spectrometry experiments.

References

1 F. Ingravallo, *Lancet*, 2020, **5**, e258.
2 X. Cao, *Nat. Rev. Immunol.*, 2020, **20**, 269–270.
3 T. T. Le, Z. Andreadakis, A. Kumar, R. G. Román, S. Tollefsen, M. Saville and S. Mayhew, *Nat. Rev. Drug Discovery*, 2020, **19**, 305–306.
4 Y. Weisblum, F. Schmidt, F. Zhang, J. DaSilva, D. Poston, J. C. C. Lorenzi, F. Muecksch, M. Rutkowska, H. H. Hoffmann, E. Michailidis, C. Gaebler, M. Agudelo, A. Cho, Z. Wang, A. Gazumyan, M. Cipolla, L. Luchsinger, C. D. Hillyer, M. Caskey, D. F. Robbiani, C. M. Rice, M. C. Nussenzweig, T. Hatziioannou and P. D. Bieniasz, *eLife*, 2020, **9**, e61312.
5 A. J. Greaney, A. N. Loes, K. H. D. Crawford, T. N. Starr, K. D. Malone, H. Y. Chu and J. D. Bloom, *Cell Host Microbe*, 2021, **29**, 463–476.
6 P. Wang, M. S. Nair, L. Liu, S. Iketani, Y. Luo, Y. Guo, M. Wang, J. Yu, B. Zhang, P. D. Kwong, B. S. Graham, J. R. Mascola, J. Y. Chang, M. T. Yin, M. Sobieszczyk, C. A. Kyratsous, L. Shapiro, Z. Sheng, Y. Huang and D. D. Ho, *Nature*, 2021, **593**, 130–135.
7 M. D. Sacco, C. Ma, P. Lagarias, A. Gao, J. A. Townsend, X. Meng, P. Dube, X. Zhang, Y. Hu, N. Kitamura, B. Hurst, B. Tarbet, M. T. Marty, A. Kolocouris, Y. Xiang, Y. Chen and J. Wang, *Sci. Adv.*, 2020, **6**, eabe0751.
8 S. Ullrich and C. Nitsche, *Bioorg. Med. Chem. Lett.*, 2020, **30**, 127377.
9 L. Zhang, D. Lin, X. Sun, U. Curth, C. Drosten, L. Sauerhering, S. Becker, K. Rox and R. Hilgenfeld, *Science*, 2020, **368**, 409–412.
10 C. M. Chu, V. C. C. Cheng, I. F. N. Hung, M. M. L. Wong, K. H. Chan, K. S. Chan, R. Y. T. Kao, L. L. M. Poon, C. L. P. Wong, Y. Guan, J. S. M. Peiris and K. Y. Yuen, *Thorax*, 2004, **59**, 252–256.
11 B. Cao, Y. Wang, D. Wen, W. Liu, J. Wang, G. Fan, L. Ruan, B. Song, Y. Cai, M. Wei, X. Li, J. Xia, N. Chen, J. Xiang, T. Yu, T. Bai, X. Xie, L. Zhang, C. Li, Y. Yuan, H. Chen, H. Li, H. Huang, S. Tu, F. Gong, Y. Liu, Y. Wei, C. Dong, F. Zhou, X. Gu, J. Xu, Z. Liu, Y. Zhang, H. Li, L. Shang, K. Wang, K. Li, X. Zhou, X. Dong, Z. Qu, S. Lu, X. Hu, S. Ruan, S. Luo, J. Wu, L. Peng, F. Cheng, L. Pan, J. Zou, C. Jia, J. Wang, X. Liu, S. Wang, X. Wu, Q. Ge, J. He, H. Zhan, F. Qiu, L. Guo, C. Huang, T. Jaki, F. G. Hayden, P. W. Horby, D. Zhang and C. Wang, *N. Engl. J. Med.*, 2020, **382**, 1787–1799.
12 P. W. Horby, M. Mafham, J. L. Bell, L. Linsell, N. Staplin, J. Emberson, A. Palfreeman, J. Raw, E. Elmahi, B. Prudon, C. Green, S. Carley, D. Chadwick, M. Davies, M. P. Wise, J. K. Baillie, L. C. Chappell, S. N. Faust, T. Jaki, K. Jefferey, W. S. Lim, A. Montgomery, K. Rowan, E. Juszczak, R. Haynes and M. J. Landray, *Lancet*, 2020, **396**, 1345–1352.
13 G. Li and E. De Clercq, *Nat. Rev. Drug Discovery*, 2020, **19**, 149–150.
14 R. Abdelnabi, C. S. Foo, D. Jochmans, L. Vangeel, S. De Jonghe, P. Augustijns, R. Mols, B. Weynand, T. Wattanakul, R. M. Hoglund, J. Tarning, C. E. Mowbray, P. Sjö, F. Escudié, I. Scandale, E. Chatelain and J. Neyts, *Nat. Commun.*, 2022, **13**, 719.
15 C. N. Morrison, K. E. Prosser, R. W. Stokes, A. Cordes, N. Metzler-Nolte and S. M. Cohen, *Chem. Sci.*, 2020, **11**, 1216–1225.
16 J. Karges, R. W. Stokes and S. M. Cohen, *Trends Chem.*, 2021, **3**, 523–534.
17 L. Feng, Y. Geisselbrecht, S. Blanck, A. Wilbuer, G. E. Atilla-Gokcumen, P. Filippakopoulos, K. Kräling, M. A. Celik, K. Harms, J. Maksimoska, R. Marmorstein, G. Frenking, S. Knapp, L. O. Essen and E. Meggers, *J. Am. Chem. Soc.*, 2011, **133**, 5976–5986.

18 E. Meggers, *Chem. Commun.*, 2009, 1001–1010.
19 E. Hillard, A. Vessières, L. Thouin, G. Jaouen and C. Amatore, *Angew. Chem., Int. Ed.*, 2006, **45**, 285–290.
20 Y. Lin, Y. C. Ong, S. Keller, J. Karges, R. Bouchene, E. Manoury, O. Blacque, J. Müller, N. Anghel, A. Hemphill, C. Häberli, A. C. Taki, R. B. Gasser, K. Cariou, J. Keiser and G. Gasser, *Dalton Trans.*, 2020, **49**, 6616–6626.
21 D. Dive and C. Biot, *ChemMedChem*, 2008, **3**, 383–391.
22 Z. Jin, X. Du, Y. Xu, Y. Deng, M. Liu, Y. Zhao, B. Zhang, X. Li, L. Zhang, C. Peng, Y. Duan, J. Yu, L. Wang, K. Yang, F. Liu, R. Jiang, X. Yang, T. You, X. Liu, X. Yang, F. Bai, H. Liu, X. Liu, L. W. Guddat, W. Xu, G. Xiao, C. Qin, Z. Shi, H. Jiang, Z. Rao and H. Yang, *Nature*, 2020, **582**, 289–293.
23 L. Sancineto, F. Mangiavacchi, A. Dąbrowska, A. Pacuła, M. Obieziurska-Fabisiak, C. Scimmi, Y. Lei, J. Kong, Y. Zhao, K. dos Santos Machado, A. V. Werhli, G. Ciancaleoni, V. Nascimento, A. Kula-Pacurar, E. J. Lenardao, H. Yang, J. Ścianowski, K. Pyrc and C. Santi, *ChemRxiv*, 2020, preprint, DOI: **10.26434/chemrxiv.12994250.v12994251**.
24 L.-Y. Sun, C. Chen, J. Su, J.-Q. Li, Z. Jiang, H. Gao, J.-Z. Chigan, H.-H. Ding, L. Zhai and K.-W. Yang, *Bioorg. Chem.*, 2021, **112**, 104889.
25 K. Amporndanai, X. Meng, W. Shang, Z. Jin, Y. Zhao, Z. Rao, Z.-J. Liu, H. Yang, L. Zhang, P. M. O'Neill and S. S. Hasnain, *Nat. Commun.*, 2021, **12**, 3061.
26 M. Gil-Moles, S. Türck, U. Basu, A. Pettenuzzo, S. Bhattacharya, A. Rajan, X. Ma, R. Büssing, J. Wölker, H. Burmeister, H. Hoffmeister, P. Schneeberg, A. Prause, P. Lippmann, J. Kusi-Nimarko, S. Hassell-Hart, A. McGown, D. Guest, Y. Lin, A. Notaro, R. Vinck, J. Karges, K. Cariou, K. Peng, X. Qin, X. Wang, J. Skiba, K. Szczupak, K. Kowalski, U. Schatzschneider, C. Hemmert, H. Gornitzka, E. R. Milaeva, A. A. Nazarov, G. Gasser, J. Spencer, L. Ronconi, U. Kortz, J. Cinatl, D. Bojkova and I. Ott, *Chem. Eur. J.*, 2021, **27**, 17928–17940.
27 J. Karges, M. Kalaj, M. Gembicky and S. M. Cohen, *Angew. Chem., Int. Ed.*, 2021, **60**, 10716–10723.
28 Z. Huang and J. J. Wilson, *Eur. J. Inorg. Chem.*, 2021, **2021**, 1312–1324.
29 K. K.-W. Lo, K. Y. Zhang and S. P.-Y. Li, *Eur. J. Inorg. Chem.*, 2011, **2011**, 3551–3568.
30 S. Hostachy, C. Policar and N. Delsuc, *Coord. Chem. Rev.*, 2017, **351**, 172–188.
31 E. B. Bauer, A. A. Haase, R. M. Reich, D. C. Crans and F. E. Kühn, *Coord. Chem. Rev.*, 2019, **393**, 79–117.
32 R. Schibli, R. La Bella, R. Alberto, E. Garcia-Garayoa, K. Ortner, U. Abram and P. A. Schubiger, *Bioconjugate Chem.*, 2000, **11**, 345–351.
33 T. R. Hayes, B. B. Kasten, C. L. Barnes and P. D. Benny, *Dalton Trans.*, 2014, **43**, 6998–7001.
34 S. Mundwiler, M. Kündig, K. Ortner and R. Alberto, *Dalton Trans.*, 2004, 1320–1328.
35 M. Schutte-Smith and H. G. Visser, *Polyhedron*, 2015, **89**, 122–128.
36 M. D. Hall, K. A. Telma, K.-E. Chang, T. D. Lee, J. P. Madigan, J. R. Lloyd, I. S. Goldlust, J. D. Hoeschele and M. M. Gottesman, *Cancer Res.*, 2014, **74**, 3913–3922.
37 M. Patra, T. Joshi, V. Pierroz, K. Ingram, M. Kaiser, S. Ferrari, B. Spingler, J. Keiser and G. Gasser, *Chem. Eur. J.*, 2013, **19**, 14768–14772.
38 W. Vuong, M. B. Khan, C. Fischer, E. Arutyunova, T. Lamer, J. Shields, H. A. Saffran, R. T. McKay, M. J. van Belkum, M. A. Joyce, H. S. Young, D. L. Tyrrell, J. C. Vederas and M. J. Lemieux, *Nat. Commun.*, 2020, **11**, 4282.
39 R. Rajaratnam, E. K. Martin, M. Dörr, K. Harms, A. Casini and E. Meggers, *Inorg. Chem.*, 2015, **54**, 8111–8120.
40 J. Maksimoska, L. Feng, K. Harms, C. Yi, J. Kissil, R. Marmorstein and E. Meggers, *J. Am. Chem. Soc.*, 2008, **130**, 15764–15765.
41 S. Gaire, B. R. Schrage and C. J. Ziegler, *Inorg. Chem.*, 2021, **60**, 10105–10108.
42 N. Saleh, M. Srebro, T. Reynaldo, N. Vanthuyne, L. Toupet, V. Y. Chang, G. Muller, J. A. G. Williams, C. Roussel, J. Autschbach and J. Crassous, *Chem. Commun.*, 2015, **51**, 3754–3757.
43 T. Ou, H. Mou, L. Zhang, A. Ojha, H. Choe and M. Farzan, *PLoS Pathog.*, 2021, **17**, e1009212.
44 D. M. Mellott, C.-T. Tseng, A. Drelich, P. Fajtová, B. C. Chenna, D. H. Kostomiris, J. Hsu, J. Zhu, Z. W. Taylor, K. I. Kocurek, V. Tat, A. Katzfuss, L. Li, M. A. Giardini, D. Skinner, K. Hirata, M. C. Yoon, S. Beck, A. F. Carlin, A. E. Clark, L. Beretta, D. Maneval, V. Hook, F. Frueh, B. L. Hurst, H. Wang, F. M. Raushel, A. J. O'Donoghue, J. Siqueira-Neto, T. D. Meek and J. H. McKerrow, *ACS Chem. Biol.*, 2021, **16**, 642–650.
45 G. Kokic, H. S. Hillen, D. Tegunov, C. Dienemann, F. Seitz, J. Schmitzova, L. Farnung, A. Siewert, C. Höbartner and P. Cramer, *Nat. Commun.*, 2021, **12**, 279.
46 A. Narayanan, M. Narwal, S. A. Majowicz, C. Varricchio, S. A. Toner, C. Ballatore, A. Brancale, K. S. Murakami and J. Jose, *Commun. Biol.*, 2022, **5**, 169.
47 A. J. Pruijssers, A. S. George, A. Schäfer, S. R. Leist, L. E. Gralinksi, K. H. Dinnon, B. L. Yount, M. L. Agostini, L. J. Stevens, J. D. Chappell, X. Lu, T. M. Hughes, K. Gully, D. R. Martinez, A. J. Brown, R. L. Graham, J. K. Perry, V. Du Pont, J. Pitts, B. Ma, D. Babusis, E. Murakami, J. Y. Feng, J. P. Bilello, D. P. Porter, T. Cihlar, R. S. Baric, M. R. Denison and T. P. Sheahan, *Cell Rep.*, 2020, **32**, 107940.